SUPPLEMENTARY TABLE

Supplementary Table S1. Pairwise comparisons of the N2D-*vs*-CTD orientation in *V. cholerae* GspE^{EpsE}, *Aa*PilT and *Pa*PilT subunits. Related to Figure 2 and 4

			*Vc*GspE				*Aa*PilT				*Pa*PilT		
			qC_6	C_2			C_6	qC_2			C_2		
				A	B	C		D	E	F	A	B	C
Vc GspE	qC_6			34.0	16.0	40.9	40.2	43.0	43.0	42.4	35.3	24.6	23.1
	C_2	A	34.0		31.5	48.4	26.0	38.8	29.4	35.6	20.7	21.5	18.8
		B	16.0	31.5		46.7	37.9	47.2	35.2	44.4	37.7	26.8	19.2
		C	40.9	48.4	46.7		27.6	14.7	73.4	17.2	30.0	30.2	38.0
Aa PilT	C_6		40.2	26.0	37.9	27.6		16.8	51.8	13.6	11.8	15.3	19.9
	qC_2	D	43.0	38.8	47.2	14.7	16.8		66.4	3.9	20.3	23.7	31.9
		E	43.0	29.4	35.2	73.4	51.8	66.4		63.2	48.3	44.0	36.1
		F	42.4	35.6	44.4	17.2	13.6	3.9	63.2		16.5	20.9	29.1
Pa PilT	C_2	A	35.3	20.7	37.7	30.0	11.8	20.3	48.3	16.5		11.0	17.7
		B	24.6	21.5	26.8	30.2	15.3	23.7	44.0	20.9	11.0		9.2
		C	23.1	18.8	19.2	38.0	19.9	31.9	36.1	29.1	17.7	9.2	

Each pairwise comparison of two subunits is based on a superposition of two CTD domains. The resultant superposition operation is applied to the entire subunit. Subsequently the two N2D domains are superimposed. The rotation angle of this second superposition is the difference in N2D-*vs*-CTD orientation given in the Table.

*Aa*PilT with C_6 hexamer symmetry (PDB: 2EWV (Satyshur et al., 2007)); *Aa*PilT with quasi-C_2 (qC_2) hexamer symmetry (PDB: 2GSZ (Satyshur et al., 2007)); *Pa*PilT with C_2 hexamer symmetry (PDB: 3JVV (Misic et al., 2010)).

SUPPLEMENTARY FIGURES

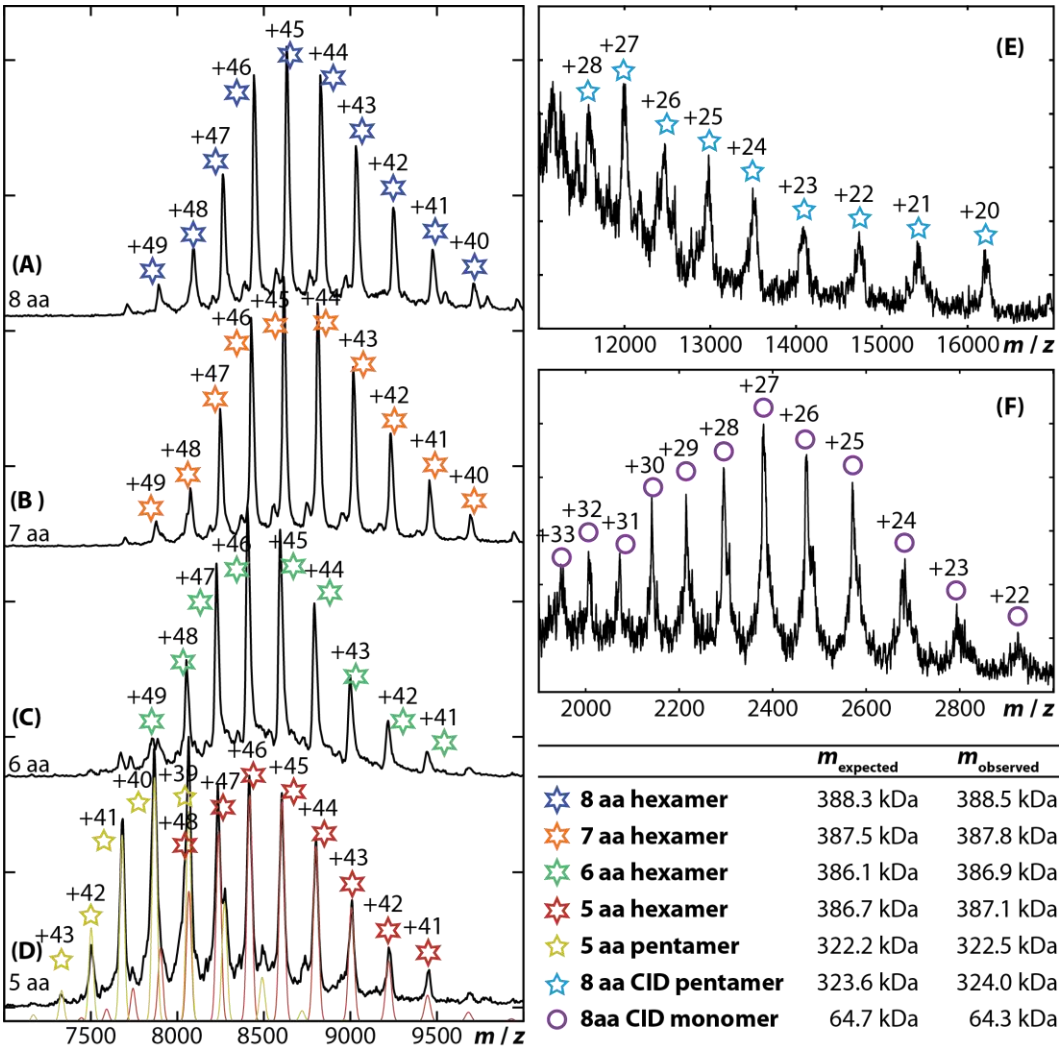

Figure S1. Oligomerization states of $^{\Delta N1}$GspE^{EpsE}-5aa-Hcp1 and $^{\Delta N1}$GspE^{EpsE}-7aa-Hcp1 from *V. cholerae* Related to Figure 1

Native mass spectra of $^{\Delta N1}$GspE^{EpsE} -8aa-Hcp1 (A), $^{\Delta N1}$GspE^{EpsE}-7aa-Hcp1 (B), and $^{\Delta N1}$GspE^{EpsE}-6aa-Hcp1 (C). The data show that these proteins can each assemble as hexamers is solution, but that $^{\Delta N1}$GspE^{EpsE}-5aa-Hcp1 (**D**) forms pentameric and hexameric complexes. Tandem mass spectra were also performed in which all ions greater than ~7500 *m/z* were isolated in the gas phase and subsequently fragmented using collision-induced dissociation. The appearance of pentamer and monomer product ions during all gas-phase CID experiments supports the assignment of hexamer precursor ions in **A**-**D**. Note that the loss of peptide ions from the precursor ions was also observed, but that fragmentation channel was less structurally informative. The measured and expected masses for all ions are reported in the table.

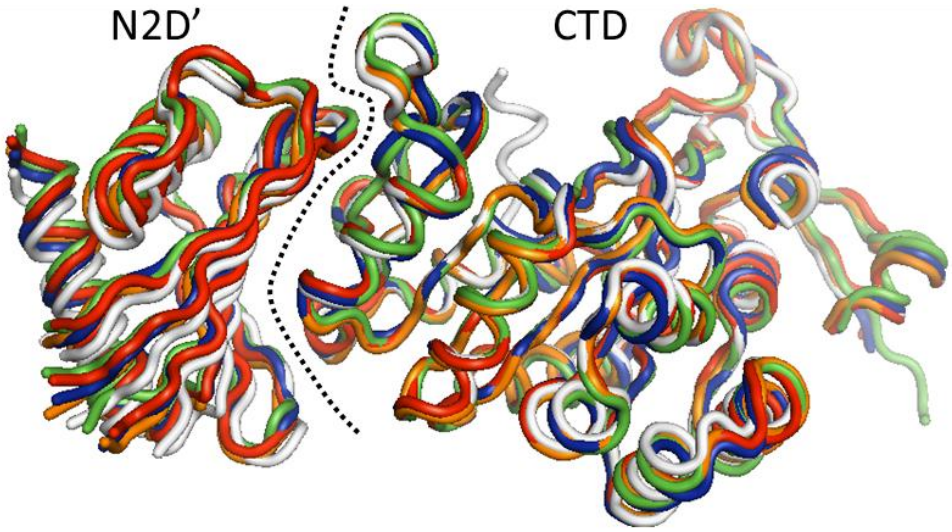

Figure S2. The CTD•N2D' construction unit in GspE^{EpsE} hexamers and the helical GspE^{EpsE} structure. Related to Figure 2

Superposition of the CTDs shows that the CTD•N2D' construction units are essentially the same for all *V. cholerae* GspE^{EpsE} structures. Depicted are: one CTD•N2D' unit from the C_6 hexamer (orange), the three independent units from the C_2 hexamer (colored blue, red and green as in Figure 2A), and the CTD•N2D' unit from the helical $^{\Delta 90}$GspE ^{EpsE} structure (grey; PDB: 1P9W (Robien et al., 2003)). The dashed line indicates the separation between the N2D' and CTD domains.

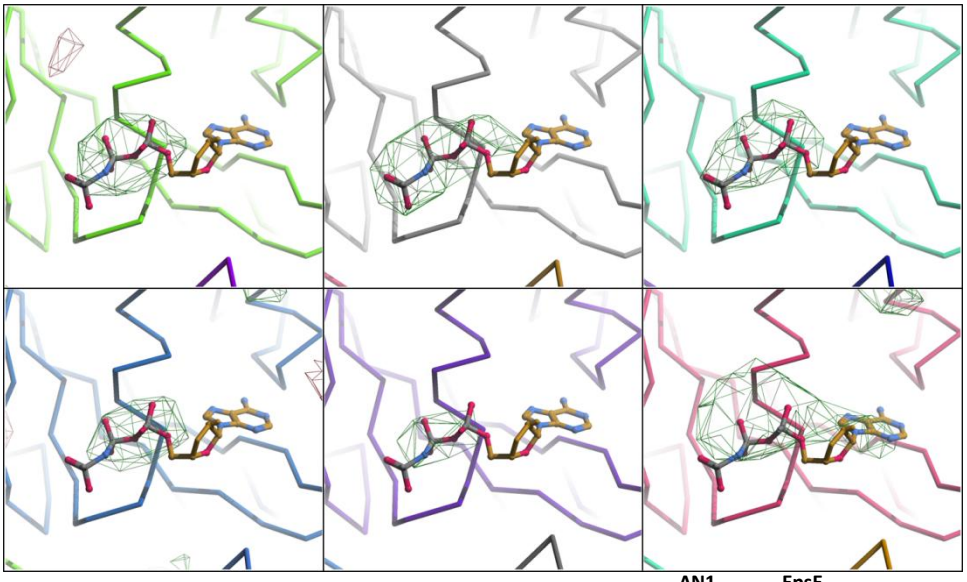

Figure S3. Electron densities of nucleotides in *V. cholerae* $^{\Delta N1}$GspE^{EpsE}-Hcp1 fusion structures. Related to Figure2 (Fobs-Fcalc) difference electron densities at the 3 sigma level are shown. The phases were obtained without including nucleotide coordinates.

Figure S3A. Electron densities at the nucleotide position in the six subunits of $^{\Delta N1}$GspE^{EpsE}-6aa-Hcp1. The nucleotides present in the protein solution were ADP and AMPPNP. Shown in each panel are: (i) the Cα traces of the six subunits in the asymmetric unit (in six different colors); (ii) AMPPNP coordinates from the $^{\Delta 90}$GspE^{EpsE} structure (PDB: 1P9W (Robien et al., 2003)) after superimposing the CTD of that structure onto the CTD of each of the six crystallographically independent subunits of the $^{\Delta N1}$GspE^{EpsE}-6aa-Hcp1 structure.

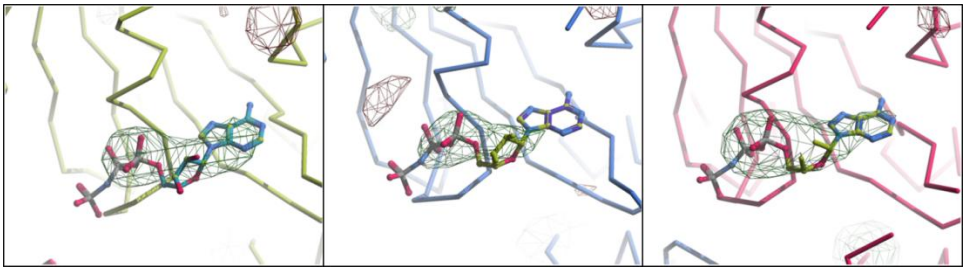

Figure S3B. Electron densities at the nucleotide position in the $^{\Delta N1}$GspE^{EpsE}-8aa-Hcp1 structure. The nucleotide present in the protein solution was ADP, $AlCl_3$, and NaF. Shown in each panel are: (i) the Cα traces of the three subunits in the asymmetric unit in three different colors; (ii) AMPPNP coordinates from the *V. cholerae* $^{\Delta 90}$GspE^{EpsE} structure (PDB: 1P9W(Robien et al., 2003)) after superimposing the CTD of that structure onto the CTD of each of the three crystallographically independent subunits from the $^{\Delta N1}$GspE^{EpsE}-8aa-Hcp1 structure.

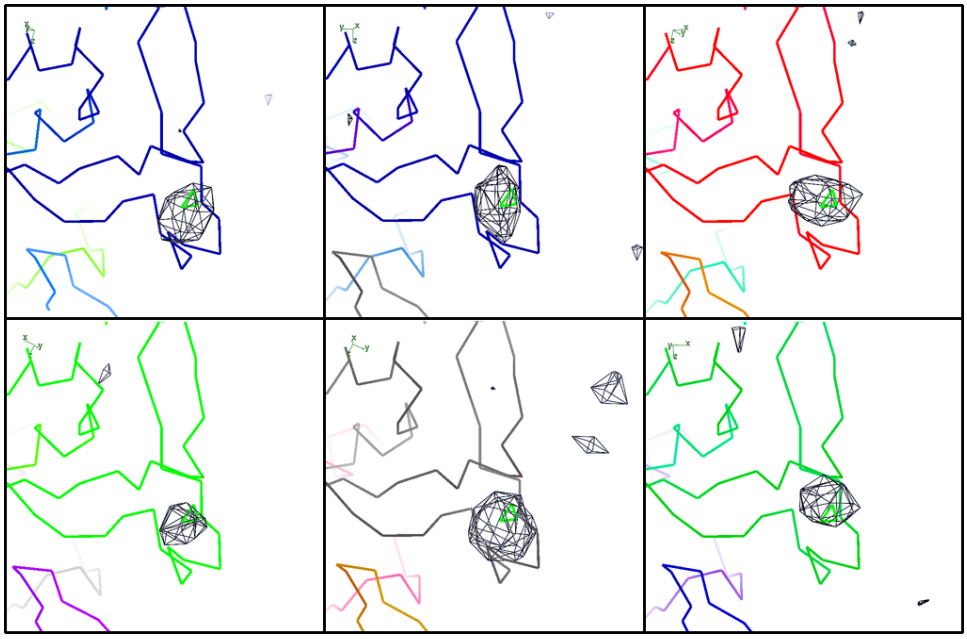

Figure S4. Anomalous electron difference densities of zinc sites in V. cholerae $^{\Delta N1}$GspE^{EpsE}-6aa-Hcp1. Related to Figure 2

The peak heights at the zinc positions (as located in the $^{\Delta 90}$GspE^{EpsE} structure (PDB: 1P9W; (Robien et al., 2003)) in the six independent crystallographic subunits of the $^{\Delta N1}$GspE^{EpsE}-6aa-Hcp1 hexamer are: 4.4, 4.5, 4.5, 4.8, 5.3 and 6.7 sigma.

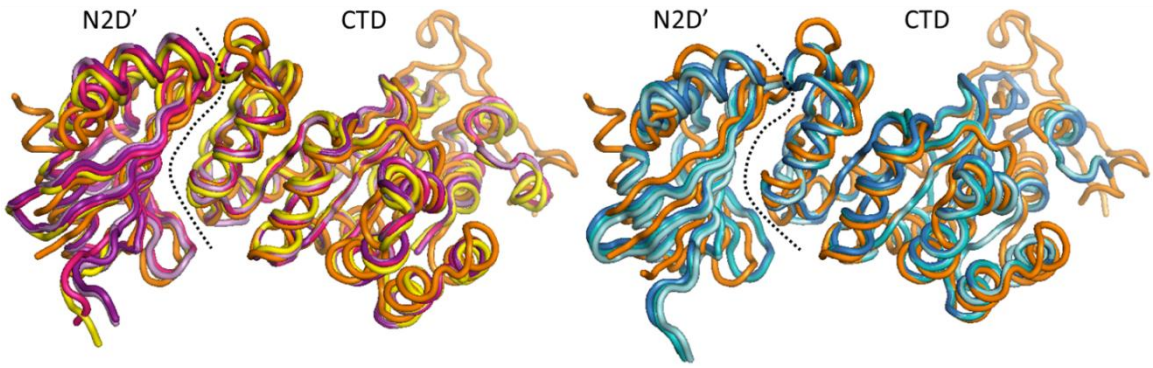

Figure S5. The CTD•N2D' construction units in GspE^{EpsE} and PilT hexamers. Related to Figure 4

The CTD•N2D' construction units of the T2SS GspE^{EpsE} ATPase and of two T4PS PilT ATPases superimpose remarkably well. The dotted line indicates the separation of the N2D' and the CTD.

Left: superposition of the CTDs of the *Aa*PilT C_6 hexamer (yellow;(Satyshur et al., 2007)) and *Aa*PilT quasi C_2 hexamer (different shades of purple) onto subunit E of the GspE^{EpsE} C_6 hexamer (orange).

Right: alignment of the CTDs of *Pa*PilT (different shades of blue;(Misic et al., 2010)) to subunit E of the GspE^{EpsE} C_6 hexamer (orange).

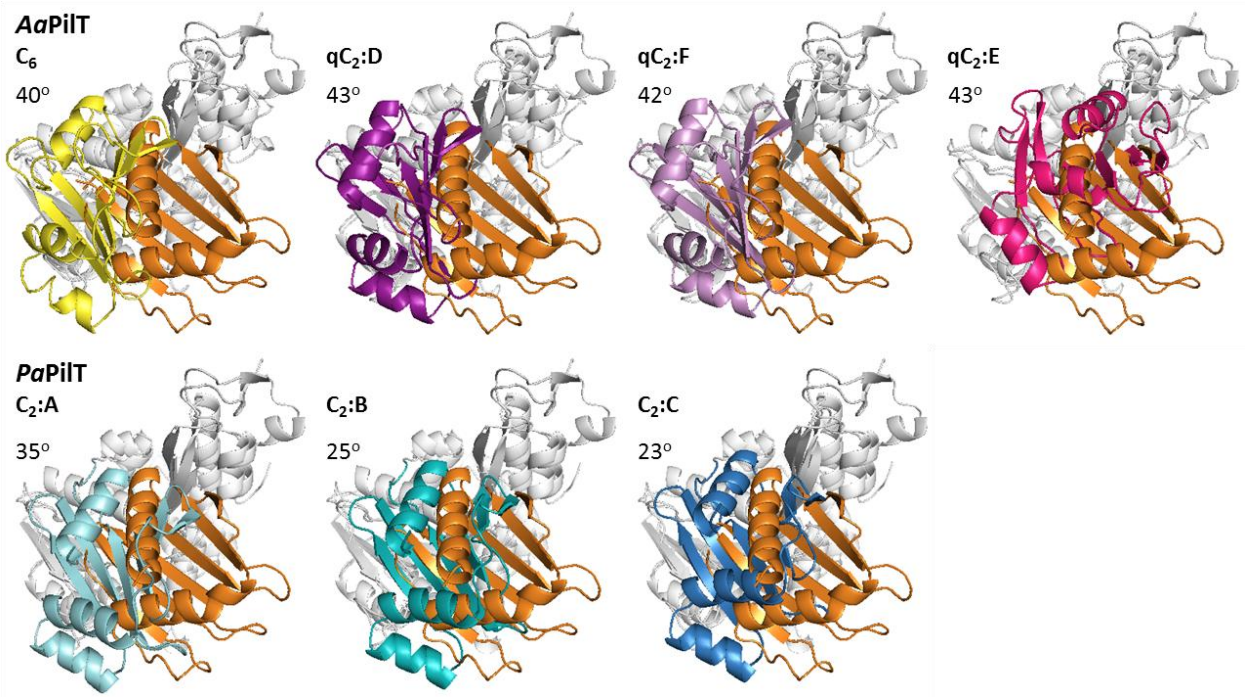

Figure S6. The variability in N2D-*vs*-CTD orientations in GspE^{EpsE} and PilT hexamers. Related to Figure4

Differences in orientation of the N2D-*vs*-CTD orientations in T2SS and T4PS ATPases, viewed with the N2D on top and the CTD below. This direction of view is approximately orthogonal to the more canonical views of Figures 2B and 4B. The superimposed CTDs of each pair of subunits are colored grey. Subunit E of the GspE^{EpsE} qC_6 hexamer (orange N2D domain) functions as reference in all figures. The difference in N2D orientation is shown in degrees in the left upper corner of each pair. Note that none of the other subunits have the "orange" N2D-*vs*-CTD orientation.

Top: superposition of the CTDs of *Aa*PilT C_6 hexamer (yellow; PDB: 2EWV) and qC_2 hexamer (different shades of purple; PDB: 2GSZ) to subunit E of the GspE^{EpsE} qC_6 hexamer (orange).
Bottom: superposition of the CTDs of *Pa*PilT C_2 hexamer (different shades of blue; PDB: 3JVV) to subunit E of the GspE^{EpsE} C_6 hexamer (orange).

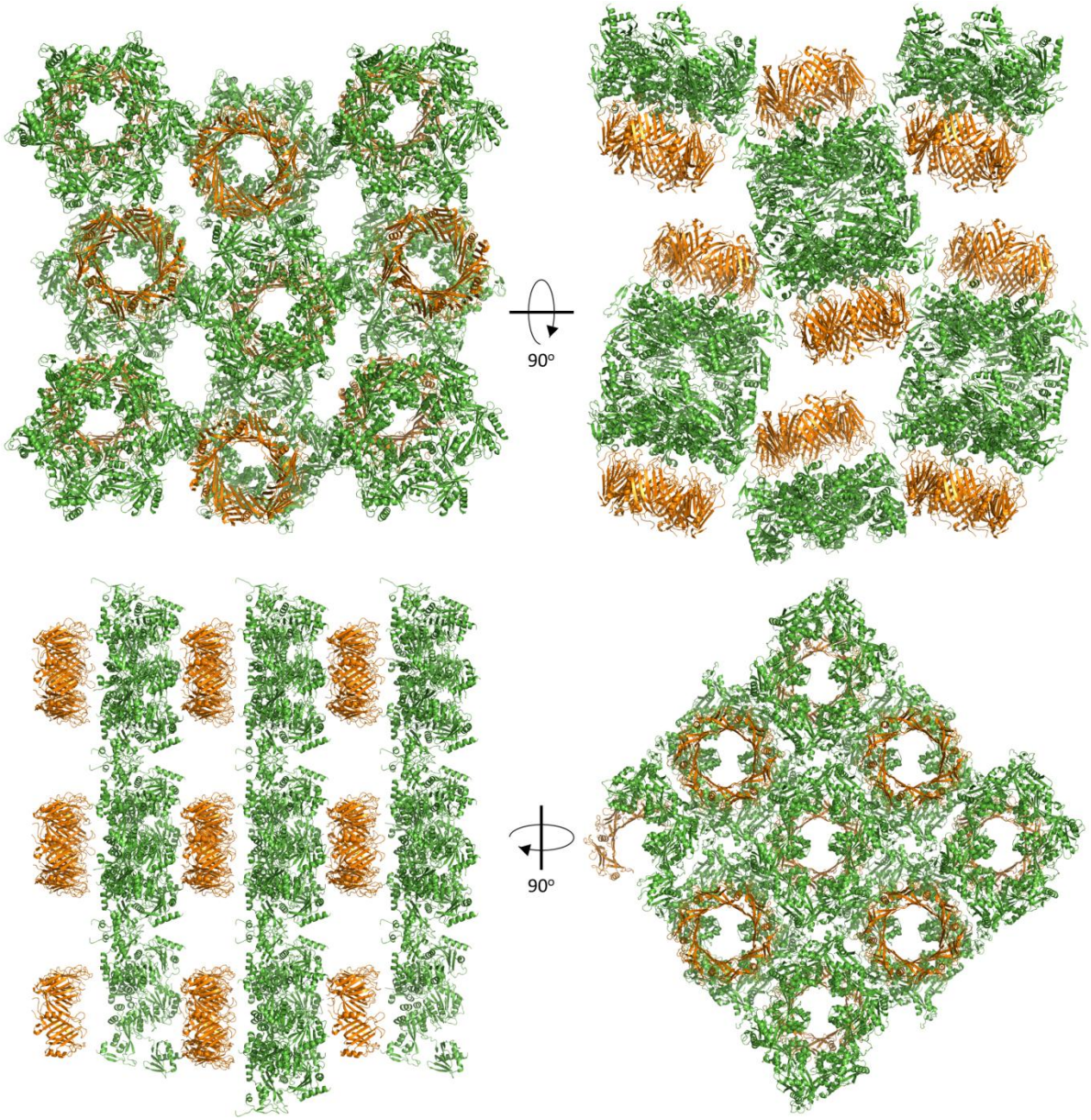

Figure S7. Crystal packing of GspE^{EpsE}-Hcp1 hexamers. Related to Figure1

Crystal packing of $^{\Delta N1}$GspE^{EpsE}-6aa-Hcp1 (top) and $^{\Delta N1}$GspE^{EpsE}-8aa-Hcp1 (bottom) with $^{\Delta N1}$GspE^{EpsE} in green and Hcp1 in orange. In the case of $^{\Delta N1}$GspE^{EpsE}-8aa-Hcp1 alternating layers of Hcp1 and $^{\Delta N1}$GspE^{EpsE} are clearly present.

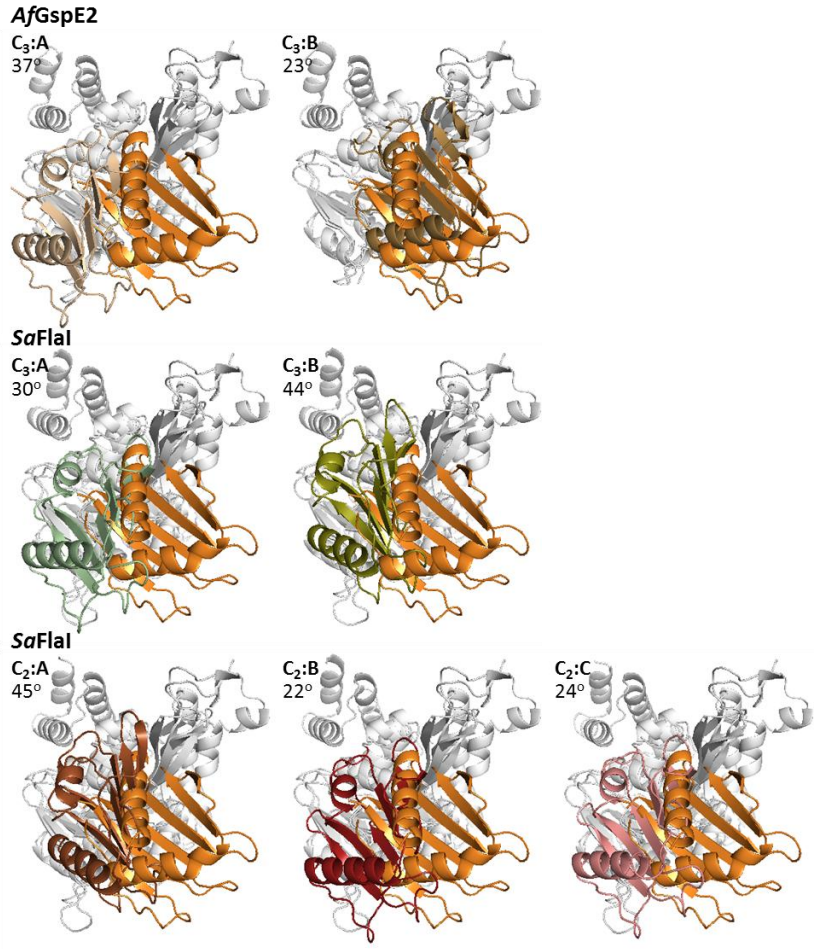

Figure S8. The variability of the N2D-*vs*-CTD orientations in *V. cholerae* GspE^{EpsE} and archaeal ATPases fom *Archaeoglobus fulgidus* (*Af*GspE2) and from *Sulfolobus acidocaldarius* (*Sa*FlaI). Related to Figure 4

Differences in orientation of the N2D-*vs*-CTD orientations in T2SS and archaeal non-T2SS ATPases, viewed with the N2D on top and the CTD below. The percentage of sequence identity per domain is given in Figure 1A. This direction of view is approximately orthogonal to the more canonical views of Figures 2B and 4B. The superimposed CTDs of each pair of subunits are colored grey. Subunit E of the GspE^{EpsE} qC_6 hexamer (orange N2D domain) functions as reference in all figures. The difference in N2D orientation is shown in degrees in the left upper corner of each pair. ((Reindl et al., 2013; Yamagata and Tainer, 2007)).

Top: superposition of the CTDs of *Af*GspE2 C_3 hexamer (different shades of brown; PDB: 2OAP (Yamagata and Tainer, 2007)) to subunit E of the GspE^{EpsE} qC_6 hexamer (orange).

Middle: superposition of the CTDs of *Sa*FlaI C_3 hexamer (different shades of green; PDB: 4II7 (Reindl et al., 2013)) to subunit E of the GspE^{EpsE} qC_6 hexamer (orange).

Bottom: superposition of the CTDs of *Sa*FlaI C_2 hexamer (different shades of red; PDB: 4II7) to subunit E of the GspE^{EpsE} qC_6 hexamer (orange).

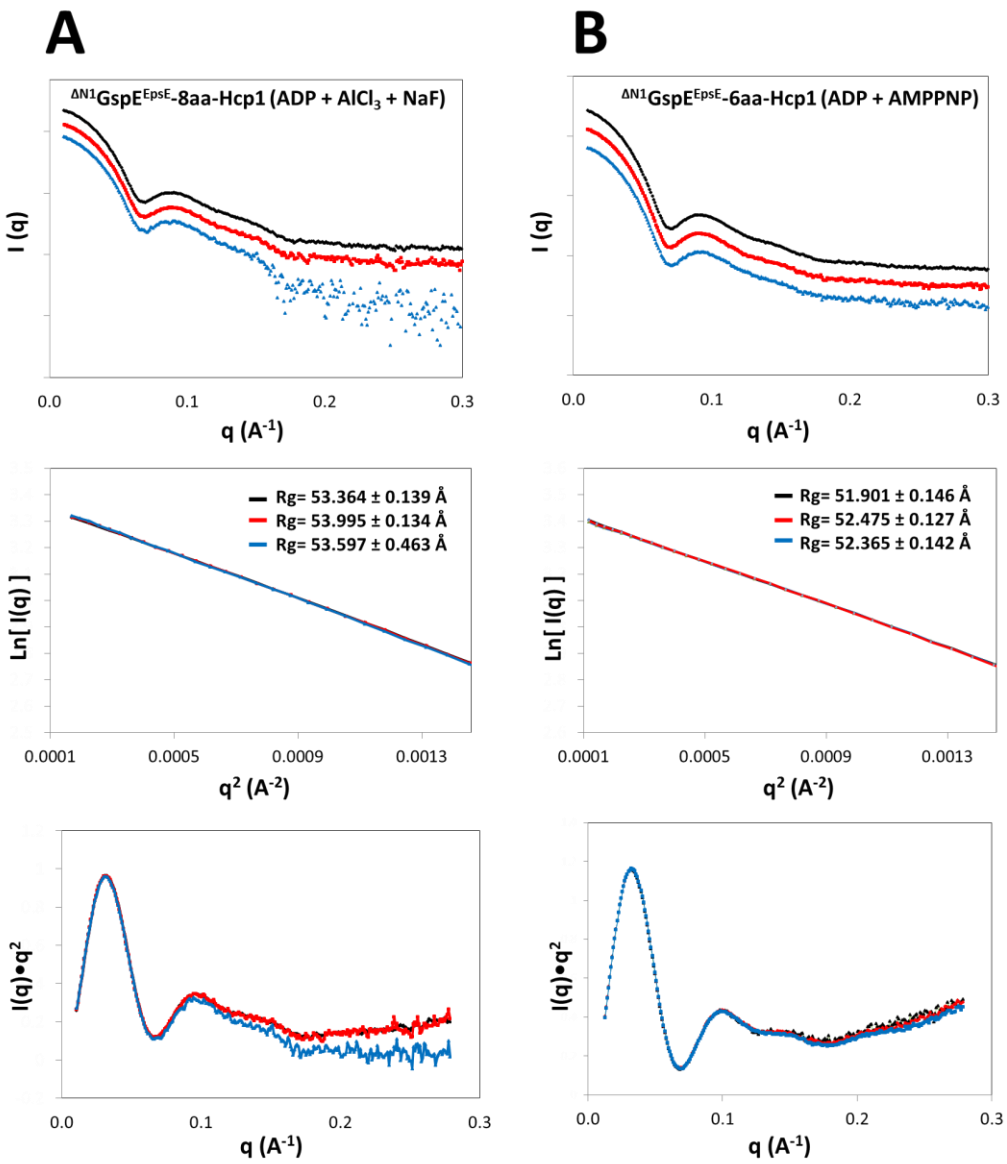

Figure S9. SAXS studies on $^{\Delta N1}GspE^{EpsE}$-6aa-Hcp1 and $^{\Delta N1}GspE^{EpsE}$-8aa-Hcp1. Related to Figure 3

The SAXS data were measured at three protein concentrations for each sample: 4.8 (black), 2.4 (red) and 1.37 (blue) mg/mL at 20 ˚C. **Top:** The raw SAXS data. Middle: **the** linearity of the Guinier region *versus* Rg (for q.Rg < 1.3). Bottom: the Kratky plots (bottom). No significant concentration dependent effects were observed.

REFERENCES

Misic, A.M., Satyshur, K.A., and Forest, K.T. (2010). P. aeruginosa PilT structures with and without nucleotide reveal a dynamic type IV pilus retraction motor. J. Mol. Biol *400*, 1011-1021.

Reindl, S., Ghosh, A., Williams, G.J., Lassak, K., Neiner, T., Henche, A.L., Albers, S.V., and Tainer, J.A. (2013). Insights into FlaI Functions in Archaeal Motor Assembly and Motility from Structures, Conformations, and Genetics. Mol. Cell *49*, 1069-1082.

Robien, M.A., Krumm, B.E., Sandkvist, M., and Hol, W.G. (2003). Crystal structure of the extracellular protein secretion NTPase EpsE of Vibrio cholerae. J. Mol. Biol *333*, 657-674.

Satyshur, K.A., Worzalla, G.A., Meyer, L.S., Heiniger, E.K., Aukema, K.G., Misic, A.M., and Forest, K.T. (2007). Crystal structures of the pilus retraction motor PilT suggest large domain movements and subunit cooperation drive motility. Structure *15*, 363-376.

Yamagata, A., and Tainer, J.A. (2007). Hexameric structures of the archaeal secretion ATPase GspE and implications for a universal secretion mechanism. The EMBO journal *26*, 878-890.